Journal of Directed Energy, **1**, Fall 2003, 73–92

Propagation of Short, High-Intensity Laser Pulses in Air

P. Sprangle,* J. R. Peñano, A. Ting, B. Hafizi,† and D. F. Gordon

Plasma Physics Division, Naval Research Laboratory, Washington, D.C. 20375

The atmospheric propagation of high-intensity, high-average-power laser beams is important for a number of directed energy applications. Linear as well as nonlinear processes affect atmospheric propagation of short, intense laser pulses. A set of equations for modeling the three-dimensional atmospheric propagation of intense short laser pulses is presented and discussed. The equations account for the linear propagation effects of dispersion, absorption, scattering, and turbulence. The nonlinear propagation effects included are transient thermal blooming, bound electron anharmonicity (optical Kerr effect), stimulated Raman scattering, ionization, plasma response (wakefields), and relativistic quiver motion. In many applications nonlinear effects, turbulence, and dispersion are important because of the short laser pulse durations and high peak intensities. The equations are used to study the propagation of a single laser pulse with peak power in the gigawatt range. Examples illustrate several important processes that would be associated with directed energy applications of intense laser beams, such as a free-electron laser with peak (average) power in the gigawatt (megawatt) range.

KEYWORDS: Atmospheric propagation, Blooming, Free-electron laser, Turbulence

Nomenclature

A	complex-valued amplitude of laser electric field
$\boldsymbol{B}$	magnetic field
$\boldsymbol{B}_L$	laser magnetic field
C_s	speed of sound
c, c_p, c_v	speed of light in free space; specific heat at constant pressure, at constant volume
$\boldsymbol{E}$	electric field
$\boldsymbol{E}_L$	laser electric field
e	base of natural logarithm
$\hat{\boldsymbol{e}}_x$	unit vector along x axis
$\hbar$	Planck's constant divided by 2π
I, I_0	laser intensity
i	$\sqrt{-1}$
$\boldsymbol{J}$	current density
K_t	thermal conductivity

Received January 30, 2003; revision received April 15, 2003.

*Corresponding author; e-mail: sprangle@ppdmail.nrl.navy.mil.

†Icarus Research, Inc., P.O. Box 30780, Bethesda, MD 20824-0780.

k, k_0	wavenumber, carrier wavenumber
l	natural numbers, 0, 1, 2, ...
l_0, L_0	inner and outer scale lengths
m	mass of an electron
n, n_0, n_2, n_K, n_R	total, linear, nonlinear, Kerr, and Raman refractive indices
n_n, n_e	neutral gas density, electron density
P	gas pressure
$\boldsymbol{P}$	polarization field
P_K, P_p, P_R	self-focusing critical power for Kerr, relativistic, and Raman
Q	Raman oscillator function
q	charge on an electron
R	gas constant
$r, \boldsymbol{r}; r_L$	spatial coordinate; laser spot size
r_e	classical electron radius
$\boldsymbol{S}$	source term in wave equation
S_z	axial Poynting flux
T	temperature
t	time variable
U_{ion}	ionization energy
$\boldsymbol{V}$	velocity
$\boldsymbol{V}_w$	wind velocity (slew)
v, v_g	velocity, group velocity
w_0	laser spot size
x	x coordinate
y	y coordinate
Z_R	Rayleigh range
z	z coordinate
$\alpha, \alpha_l; \alpha_{\text{ext}}$	absorption coefficient, dispersion coefficient; extinction coefficient
$\beta_l, \beta_{\text{recom}}$	dispersion parameter, recombination rate
β_g	group velocity/c
Γ	damping rate
γ	ratio of specific heats
ΔK	wavenumber mismatch
$\Delta\Omega$	frequency mismatch
δn_e	plasma density perturbation
$\delta n_T, \delta n_{\text{TB}}$	contribution to refractive index due to turbulence, thermal blooming
λ	wavelength
ν_e, ν_{ion}	electron collision frequency, ionization rate
ρ	mass density
$\rho_c, \rho_{\text{wander}}$	laser spot size spread, laser beam wander
τ	$= t - z/v_g$, retarded time
χ_L	susceptibility
ψ	phase
Ω	transition frequency
$\omega; \omega_0, \omega_p, \omega_R$	frequency; carrier frequency, plasma frequency, rotational frequency
∇	gradient operator
$\nabla_\perp^2$	transverse Laplacian operator

1. Introduction

The ability to project significant energy on a target is central to many applications of high-power lasers. These applications include countermeasures and directed energy weapons. There are a number of issues for the practical realization of these applications, including suitable laser technology, propagation, and target lethality. While technically challenging, there does not appear to be a fundamental barrier to constructing a laser system with the desired characteristics. Observations of long-distance propagation, filamentation, white light, and subterahertz radiation generation[9,11,13,16,19,20,22,23,29,31,32,44–46,48–51] in recent high-intensity, short-pulse experiments indicate the significant role played by nonlinear and dispersive effects. For a megawatt-class free-electron laser (FEL) based, for example, on a radio frequency linac configuration, the peak power (intensity) can be $\sim 10^3\times$ larger than the average. In this case nonlinear atmospheric propagation processes and dispersion are expected to be important. The subject of this paper is the analysis of the interplay between these diverse processes as they relate to the propagation of intense, high-power laser beams in the atmosphere.

Studies of laser beam propagation in the atmosphere have been performed since the advent of lasers. The development of shorter-pulse, higher-power lasers is one of the key drivers in this arena. In the 1980s most experiments were performed with lasers with pulse lengths in the nanosecond regime. In this regime, processes such as rotational Raman scattering, turbulence, and thermal blooming limit propagation in the atmosphere. These processes affect the picosecond-to-femtosecond-long laser beams, which are now available, very differently. The development of high-power FELs, similar to that at the Thomas Jefferson National Laboratory (TJNL),[28] has also motivated studies of nonlinear laser propagation effects in air.

Propagation of intense laser beams in the atmosphere is affected by a number of linear and nonlinear processes. Diffraction is a linear process by which a laser beam spreads transversely over propagation distances on the order of a Rayleigh range $Z_R = \pi w_0^2/\lambda$, where λ is the wavelength of the radiation and w_0 is the waist of the beam. Dispersion is a linear process that can result in compression, spreading, or, more generally, longitudinal pulse distortion.[1] Local fluctuations in the air density due to atmospheric turbulence affect laser beam propagation principally through the linear refractive index. These fluctuations introduce a corresponding phase variation across the wavefronts that adversely affects the coherence properties of the laser beam.[10,12,14,15,18] Linear processes can be compensated for to a great extent by employing adaptive optical elements.[4]

Nonlinear processes, such as thermal blooming and optical Kerr effect, are of special concern since they can be only partially compensated for by adaptive optics. Propagation of a laser beam in air results in a small fraction of the energy being absorbed. The absorbed energy locally heats the air and leads to a decrease in the density. This in turn lowers the refractive index and thus defocuses (blooms) the beam.[6,7,34,47] The nonlinearity leading to thermal blooming is on a macroscopic scale, involving the absorption of energy from the laser and the resulting hydrodynamic response of the air. In the case of the optical Kerr effect it is the nonlinear, anharmonic motion of bound electrons that leads to modification of the refractive index n (Refs. 1, 8, 33, 35, 36, 38, and 39). In the Kerr effect the refractive index may be written as $n = n_0 + n_K I$, where n_0 is the linear index, n_K is the Kerr contribution to the index, and I is the intensity. Since the intensity of a laser beam is typically peaked along the axis of propagation, the effective radial variation of the refractive index tends to focus the beam. If the power exceeds a critical value given by $P_K = \lambda^2/(2\pi n_0 n_K)$

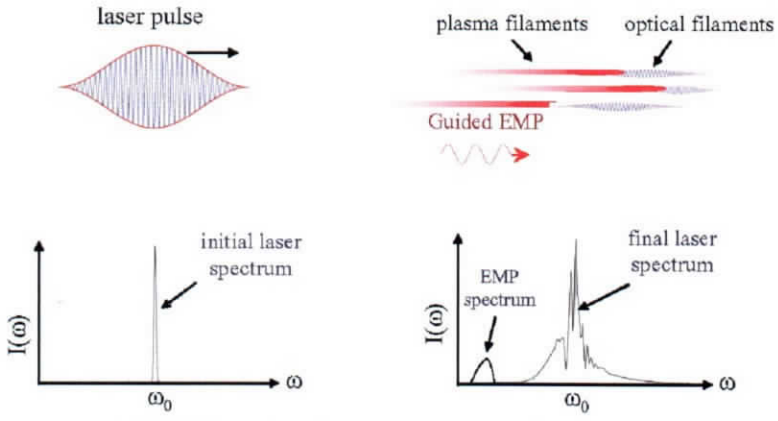

Fig. 1. Schematic depicting several processes associated with propagation of a short, intense laser pulse in the atmosphere. These include breakup of laser pulse into light filaments and generation of plasma filaments and low-frequency EMP emission.

self-focusing can be catastrophic. This is accompanied by an increase in intensity that can eventually lead to ionization of the air and formation of a plasma column. The dielectric properties of the plasma are such as to defocus the laser beam. If the focusing due to the Kerr effect is in balance with the defocusing due to the plasma, the laser pulse can be guided over an extended distance. The resulting guided optical filament can propagate far beyond the Rayleigh range. However, nonlinear processes, including generation of harmonics[2,3] and of low-frequency radiation,[16,31,50] modify the spectrum of the laser pulse considerably. A schematic depicting some of the processes associated with intense laser propagation in air is shown in Fig. 1.[40]

The characteristics of the laser source play a central role in the propagation process. FELs have the potential of generating high peak power as well as high average power, with wide flexibility in pulse format. Additionally, since FELs are in principle continuously tunable, they are suitable for use in the maritime environment, by selecting an appropriate atmospheric transmission window. There are several wavelength bands with relatively small absorption, and an FEL operating at, for instance, ~ 1 μm would appear to be a suitable candidate. Examination of the transmission windows reveals that there is, for example, a group of absorption lines of water vapor molecules at 1.152277, 1.152319, 1.152373, 1.152420, 1.152423 μm, ..., with a fractional wavelength separation $\sim 10^{-4}$. The linewidth of a picosecond-long FEL pulse is $\sim 10^{-3}$. Such a Fourier transform-limited laser pulse is likely to be modified by the presence of absorption lines of the constituents of air. In the case of an intense laser pulse, nonlinear effects, which include rotational Raman scattering, can broaden the spectrum well beyond the transform-limited width.

The primary goal of this paper is to analyze and discuss laser beam propagation in the atmosphere,[24–27,40] providing a significantly more sophisticated model than earlier studies. A three-dimensional (3D), nonlinear propagation equation is derived that incorporates the effects of diffraction, dispersion, group velocity dispersion (GVD), scattering, ionization and plasma formation, pulse energy depletion due to ionization, nonlinearities associated with bound electrons (optical Kerr effect), spatial inhomogeneity, plasma wakefields, and relativistic electron motion. For the shorter pulses and the intensities of interest, collisional

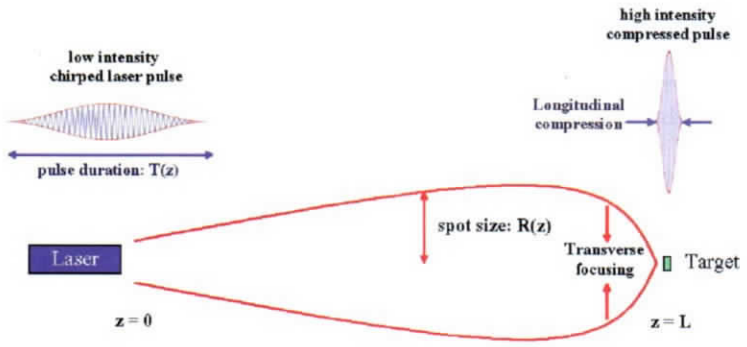

Fig. 2. Laser pulse propagating in air and impinging on a distant target. The initially chirped laser pulse undergoes longitudinal compression, while the optical Kerr process leads to transverse focusing. The combined effect is to deliver an intense pulse on target.

ionization is negligible compared to photoionization (principally multiphoton) and relativistic effects are small. In addition, stimulated molecular Raman scattering, atmospheric turbulence, and transient thermal blooming processes are incorporated into our model. While the latter processes had a significant impact on the nanosecond-scale laser pulse propagation experiments of the 1980s, today's single picosecond-to-femtosecond-scale pulses tend to be less susceptible to these. GVD, which leads to a variation of group velocity for different Fourier components of the pulse, can be severe for the shorter pulses. In fact, if the laser pulse is initially chirped, the GVD associated with air can induce a significant longitudinal compression of the pulse. By proper choice of parameters, pulse compression and nonlinear self-focusing can be arranged to occur simultaneously at a distance, creating atmospheric breakdown (spark) as indicated in Fig. 2.

This paper is organized as follows. The formulation is presented in Sec. 2, the central result being a 3D nonlinear equation describing the propagation of a laser pulse in the atmosphere. A discussion of the key processes affecting short-pulse, intense laser beam propagation in the atmosphere is given in this section. Generation of subterahertz radiation from femtosecond optical filaments in air is discussed in Sec. 3. Discussion of filament formation and guided propagation of laser energy is presented in Sec. 4. Concluding remarks are presented in Sec. 5.

2. Propagation of Intense Laser Pulses in the Atmosphere

In this section a general 3D nonlinear atmospheric propagation equation for high-intensity laser pulses is presented and discussed. The need for such a model is dictated by the fact that in recent experiments, as well as proposed megawatt-class FEL-based experiments, nonlinear as well as dispersive effects can be the dominant physical processes. This is a key difference from the laser propagation experiments of the 1980s. The shorter, more intense pulses available today and in the near future probe an entirely different regime, leading to new phenomena associated with propagation of high-intensity laser pulses.

The starting point is the wave equation for the laser electric field $\boldsymbol{E}_L(\boldsymbol{r}, t)$, given by

$$\left(\nabla_\perp^2 + \frac{\partial^2}{\partial z^2} - \frac{1}{c^2}\frac{\partial^2}{\partial t^2}\right)\boldsymbol{E}_L = \boldsymbol{S}_L + \boldsymbol{S}_{\mathrm{NL}}, \tag{1}$$

where $\nabla_\perp^2$ is the transverse Laplacian operator and z is the coordinate in the direction of propagation. The linear and nonlinear source terms in the wave equation, S_L and S_{NL}, respectively, represent the physical processes that are relevant to laser pulse propagation in the atmosphere. In the following the contributions to the source terms are enumerated and discussed.[40]

The laser electric field $\boldsymbol{E}_L(x, y, z, t)$, linear source term $\boldsymbol{S}_L(x, y, z, t)$, and nonlinear source term $\boldsymbol{S}_{NL}(x, y, z, t)$, are written in terms of complex amplitudes, $A(x, y, z, t)$, $S_L(x, y, z, t)$, and $S_{NL}(x, y, z, t)$ and a rapidly varying phase, $\psi(z, t)$, that is,

$$\boldsymbol{E}_L(x, y, z, t) = A(x, y, z, t)\exp[i\psi(z, t)]\hat{\boldsymbol{e}}_x/2 + \text{c.c.}, \tag{2a}$$

$$\boldsymbol{S}_L(x, y, z, t) = S_L(x, y, z, t)\exp[i\psi(z, t)]\hat{\boldsymbol{e}}_x/2 + \text{c.c.}, \tag{2b}$$

$$\boldsymbol{S}_{NL}(x, y, z, t) = S_{NL}(x, y, z, t)\exp[i\psi(z, t)]\hat{\boldsymbol{e}}_x/2 + \text{c.c.}, \tag{2c}$$

where $\psi(z, t) = k_0 z - \omega_0 t$ is the phase, k_0 is the carrier wavenumber, ω_0 is the carrier frequency, $\hat{\boldsymbol{e}}_x$ is a transverse unit vector in the direction of polarization, and c.c. denotes the complex conjugate. Substituting the field and source representations given by Eqs. (2) into Eq. (1) yields

$$\left(\nabla_\perp^2 - k_0^2 + \frac{\omega_0^2}{c^2} + 2ik_0\frac{\partial}{\partial z} + 2i\frac{\omega_0}{c}\frac{\partial}{\partial t} + \frac{\partial^2}{\partial z^2} - \frac{1}{c^2}\frac{\partial^2}{\partial t^2}\right)A(\boldsymbol{r}, t) = S_L(\boldsymbol{r}, t) + S_{NL}(\boldsymbol{r}, t), \tag{3}$$

where the rapidly varying phase factor has been canceled from both sides of the equation. Although the atmospheric density is spatially varying, the wavenumber is taken to be constant since the maximum change in the linear refractive index, i.e., fractional change in wavenumber, from sea level to vacuum is $\leq 10^{-4}$.

To solve Eq. (3) it is necessary to specify the various source terms. The linear source term represents the effects of dispersion, turbulence, absorption, and scattering. The physical processes underlying the nonlinear source term are more varied. The nonlinear effects included here arise from thermal blooming, bound electron (optical Kerr) motion, rotational Raman scattering, plasma, wakefield excitation, relativistic quiver motion, and ionization.

2.1. Linear source terms

The linear source term amplitude can be written as

$$S_L(\boldsymbol{r}, t) = S_D + S_T, \tag{4}$$

where S_D and S_T represent the effects of dispersion and turbulence, respectively, and are described in the following.

2.1.1. Dispersion. The linear source amplitude can be expressed as[1]

$$S_D(\boldsymbol{r}, t) = \left(\frac{\omega_0}{c}\right)^2 \sum_{\ell=0}^{\infty} i^\ell \alpha_\ell(\boldsymbol{r})\omega_0^{-\ell}\frac{\partial^\ell A(\boldsymbol{r}, t)}{\partial t^\ell}, \tag{5}$$

where $\ell = 0, 1, 2, \ldots$. The unitless dispersion coefficients $\alpha_\ell(\boldsymbol{r})$ in Eq. (5) are given by

$$\alpha_\ell = -\frac{\omega_0^{\ell-2}}{\ell!}\frac{\partial^\ell}{\partial\omega_0^\ell}\left[c^2\beta^2(\omega_0) - \omega_0^2\right], \tag{6}$$

where $\beta(\omega) = (\omega/c)[1 + 4\pi\chi_L(\omega)]^{1/2} = (\omega/c)n_0(\omega)$, $\chi_L(\omega)$ is the linear susceptibility of bound electrons, and $n_0(\omega)$ is the linear refractive index.

2.1.2. Turbulence, absorption, and scattering. Atmospheric turbulence affects the propagation of a laser beam through fluctuations in the linear refractive index.[10,12,14,15,18] The source term for turbulence can be written as

$$S_T(\boldsymbol{r}, t) = -2n_0\left(\frac{\omega_0}{c}\right)^2 \delta n_T(\boldsymbol{r})A(\boldsymbol{r}, t), \tag{7}$$

where δn_T represents the change in the linear refractive index due to turbulence. Modeling of turbulence is implemented by introducing fictitious phase screens at regular intervals $z_{n+1} = z_n + \Delta z$ along the propagation direction.[14] The screens randomize the phase of the laser field and represent the integrated effect of turbulence on propagation from z_n to z_{n+1}.

A number of other processes can be modeled on the same footing as turbulence since their effects can be represented through a modification to the linear refractive index. Absorption and scattering by the constituents of air (i.e., molecules, aerosols, etc.) are the two main processes and are particularly important in the maritime environment.[42] Absorption leads to loss of laser energy, and scattering leads to directional redistribution of laser energy and hence loss of intensity. Scattering is a strong function of the relative size of the scatterer and the laser wavelength. Two well-known limits of scattering are Rayleigh scattering ($\lambda \gg$ size of scatterer) and Mie scattering ($\lambda \sim$ size of scatterer). Conventionally, the total attenuation due to these processes is represented by a single parameter, α_{ext}, the extinction coefficient.

The combined effect of turbulence, absorption, and scattering may be modeled by assuming that the laser field amplitude evolves according to the prescription

$$A_{n+1}(x, y, \tau) = \exp\left(-\frac{1}{2}\alpha_{\text{ext}}\Delta z\right)\exp\left(\frac{i}{4}k_0^{-1}\Delta z\nabla_\perp^2\right)\exp[i\theta(x, y, z_n)]$$
$$\times \exp\left(\frac{i}{4}k_0^{-1}\Delta z\nabla_\perp^2\right)A_n(x, y, \tau), \tag{8a}$$

where

$$\theta(x, y, z_n) = k_0\int_{z_n}^{z_{n+1}} \mathrm{d}z'\delta n_T(x, y, z') \tag{8b}$$

is the random phase screen. Conventionally this is expressed as

$$\theta_n(x, y, z) = \frac{k_0 L}{\sqrt{2\pi}}\Delta z^{1/2}\int_{-\infty}^{\infty}\mathrm{d}k_x e^{ik_x x}\int_{-\infty}^{\infty}\mathrm{d}k_y e^{ik_y y}a(k_x, k_y)\Phi_n^{1/2}(k_x, k_y, z), \tag{8c}$$

where $a(k_x, k_y)$ is a complex-valued random function with Gaussian statistics, zero mean, and unit variance and $\Phi_n(k_x, k_y, z)$ is the spectral density function associated with the refractive index fluctuation δn_T. Various models for the spectral density function are available. The pure power-law (Kolmogorov) spectrum is given by

$$\Phi_n(k_x, k_y) = 0.033C_n^2\left(k_x^2 + k_y^2\right)^{-11/6}, \tag{9}$$

where C_n^2 is the refractive index structure constant. In the case of moderate turbulence $C_n^2 \sim 10^{-14}$ m$^{-2/3}$. Another commonly used model is a modified von Kármán spectral

density function

$$\Phi_n(k_x, k_y) = 0.033C_n^2\left[(2\pi/L_0)^2 + k_x^2 + k_y^2\right]^{-11/6} \exp\left[-\left(k_x^2 + k_y^2\right)\ell_0^2/35\right], \tag{10}$$

where L_0 is the outer scale length and ℓ_0 is the inner scale length. Typical values for these scale lengths are 10 m and 1 cm, respectively. However, these values can vary greatly with atmospheric conditions.

Turbulence can lead to both spreading and wandering of the laser beam. Spreading occurs in the limit where the beam spot size is large compared with the scale size of turbulence. In the opposite limit, beam wander predominates. The spreading effect of turbulence on the laser beam can be quantified in terms of the spreading angle Θ_{spread}. This is given by

$$\Theta_{\text{spread}} = \left[\left(\frac{\lambda}{\pi w_0}\right)^2 + \left(\frac{\lambda}{\pi\rho_c}\right)^2\right]^{1/2}. \tag{11}$$

The first term in this expression represents beam divergence due to diffraction, and the second is due to turbulence, where the transverse coherence distance is given by

$$\rho_c = 0.185\lambda^{6/5}\left[\int_0^L dz C_n^2(z)\right]^{-3/5} \approx 0.185\lambda\left(\frac{\lambda^{1/3}}{C_n^2 L}\right)^{3/5}. \tag{12}$$

It follows that the relative importance of turbulence and diffraction in beam spreading is determined by the relative magnitudes of the coherence length ρ_c and the spot size w_0. As an example, the coherence distance of a 1-μm laser beam over a propagation distance $L = 10$ km in an atmosphere with $C_n^2 = 10^{-14}$ m$^{-2/3}$ (moderate turbulence) is $\rho_c = 1.2$ cm and the scattering angle $\lambda/\pi\rho_c = 27$ μrad.

In addition to beam spreading, turbulence also causes the beam centroid to wander transversely according to[5]

$$\rho_{\text{wander}} \approx 1.1\left(\frac{L}{w_0}\right)\left(\frac{C_n^2 L}{w_0^{1/3}}\right)^{1/2} w_0. \tag{13}$$

Equation (13) applies to a focused beam and assumes that C_n^2 is independent of path length. As an example, the centroid of a 1-μm laser beam with spot size $w_0 = 1$ m propagating a distance $L = 10$ km in an atmosphere with $C_n^2 = 10^{-14}$ m$^{-2/3}$ (moderate turbulence) wanders, on average, a distance $\rho_{\text{wander}} = 11$ cm.

2.2. Nonlinear source terms

The nonlinear source amplitude is due to a number of effects and can be written as

$$S_{\text{NL}}(\boldsymbol{r}, t) = S_{\text{TB}} + S_{\text{Kerr}} + S_{\text{Raman}} + S_{\text{plasma}} + S_{\text{wake}} + S_{\text{rel}} + S_{\text{ion}}, \tag{14}$$

where the individual contributions are described as follows.

2.2.1. Transient thermal blooming. The heating that accompanies laser beam propagation in air changes the refractive index by an amount δn_{TB} (Refs. 6, 7, 34, and 47). A local decrease in the index leads to defocusing, or blooming, of the beam. The source term

for transient thermal blooming can be written as

$$S_{\mathrm{TB}}(\boldsymbol{r}, t) = -2n_0\left(\frac{\omega_0}{c}\right)^2 \delta n_{\mathrm{TB}}(\boldsymbol{r})A(\boldsymbol{r}, t), \tag{15}$$

where δn_{TB} represents the change in the linear refractive index due to thermal blooming. The variation in the refractive index is given by

$$\delta n_{\mathrm{TB}} = (n_0 - 1)\delta\rho/\rho_0, \tag{16}$$

where n_0 and ρ_0 are the ambient refractive index and mass density, respectively, and $\delta\rho$ is the perturbed mass density. The perturbed mass density may be obtained by employing a hydrodynamic description of air. In this case, analysis of thermal blooming starts with the continuity equation $\partial\rho/\partial t + \nabla\cdot(\rho\boldsymbol{V}) = 0$, the momentum equation $\rho\partial\boldsymbol{V}/\partial t + \rho\boldsymbol{V}\cdot\nabla\boldsymbol{V} = -\nabla P$, the energy equation $\rho c_p(\partial T/\partial t + \boldsymbol{V}\cdot\nabla T) - K_t\nabla^2 T - \partial P/\partial t - \boldsymbol{V}\cdot\nabla P = \alpha I$, and the ideal gas law $P = R\rho T$. Here, $\boldsymbol{V}$ is the fluid velocity, T is the temperature, P is the pressure, I is the laser intensity, α is the total absorption coefficient, K_t is the thermal conductivity, $R = c_p - c_v$ is the universal gas constant, and $c_p(c_v)$ is the specific heat at constant pressure (volume). To obtain the perturbed density the fluid quantities Q are expanded about their ambient values, $Q = Q_0 + \delta Q$. Linearization of the fluid equations leads to

$$\left[\rho_0 c_v\left(\frac{\partial}{\partial t} + \boldsymbol{V}_w\cdot\nabla\right) - K_t\nabla^2\right]\delta T - \frac{C_s^2}{\gamma}\left(\frac{\partial}{\partial t} + \boldsymbol{V}_w\cdot\nabla\right)\delta\rho = \alpha I, \tag{17a}$$

$$\left[\left(\frac{\partial}{\partial t} + \boldsymbol{V}_w\cdot\nabla\right)^2 - \frac{C_s^2}{\gamma}\nabla^2\right]\delta\rho = \frac{C_s^2}{\gamma}\frac{\rho_0}{T_0}\nabla^2\delta T, \tag{17b}$$

where $\boldsymbol{V}_w$ is the wind velocity (slew), $C_s = (\gamma R T_0)^{1/2}$ is the speed of sound, and $\gamma = c_p/c_v$ is the ratio of specific heats.

2.2.2. Optical Kerr (bound electron) effect. The nonlinear contribution from bound electrons, Kerr effect, is given by

$$S_{\mathrm{Kerr}}(\boldsymbol{r}, t) = \frac{\omega_0^2 n_0^2 n_K}{4\pi c}|A(\boldsymbol{r}, t)|^2 A(\boldsymbol{r}, t), \tag{18}$$

where n_K is the electronic contribution to the nonlinear refractive index. The nonlinear index defines a nonlinear self-focusing power,[8,33,35,36] $P_K = \lambda_0^2/(2\pi n_0 n_K)$.

2.2.3. Stimulated rotational Raman scattering. The source term due to stimulated molecular Raman scattering is given by[17,21]

$$S_{\mathrm{Raman}}(\boldsymbol{r}, t) = -4\pi\frac{\omega_0^2}{c^2}\chi_L Q(t)A(\boldsymbol{r}, t), \tag{19}$$

where χ_L is the linear susceptibility evaluated at frequency ω_0 and the unitless Raman oscillator function $Q(t)$ is given by

$$Q(\boldsymbol{r}, t) = \frac{n_R n_0}{2\pi\chi_L}\int_{-\infty}^{t} \mathrm{d}t'\left(\frac{\omega_R^2 + \Gamma_2^2}{\omega_R}\right)\exp[-\Gamma_2(t - t')]\sin[\omega_R(t - t')]I(\boldsymbol{r}, t'), \tag{20}$$

where ω_R ($\sim 10^{13}$ s^{-1}) is the rotational frequency and Γ_2 ($\sim 10^{10}$ s^{-1}) is the transition linewidth. The values quoted for ω_R and Γ_2 are typical of long laser pulses at a wavelength

of 1 μm. The total nonlinear refractive index is expressible as $n_{\rm NL} = n_K I + n_R$, where $n_R = 2\pi\chi_L Q(\boldsymbol{r}, t)/n_0$ is the Raman contribution to the refractive index. In the short-pulse (~femtosecond) limit, $n_R \to 0$ and $n_{\rm NL}$ is due mainly to the electronic response (Kerr effect).

2.2.4. Plasma. The plasma source term is given by[40]

$$S_{\rm plasma}(\boldsymbol{r}, t) = \frac{\omega_p^2(\boldsymbol{r}, t)}{c^2}(1 - i\nu_e/\omega_0)A(\boldsymbol{r}, t), \tag{21}$$

where $\omega_p(\boldsymbol{r}, t) = [4\pi q^2 n_e(\boldsymbol{r}, t)/m]^{1/2}$ is the plasma frequency, n_e is the plasma density generated by ionization, and ν_e is the electron collision frequency. Ionization results in a plasma column that is localized to the laser axis. The plasma column causes a local decrease in the refractive index that can defocus the laser pulse. The term proportional to the electron collision frequency is responsible for the collisional absorption of laser energy, i.e., inverse bremsstrahlung.

2.2.5. Wakefield excitation. The source term $S_{\rm wake}$ is due to the possible generation of plasma waves and is given by[40]

$$S_{\rm wake}(\boldsymbol{r}, t) = \frac{\omega_p^2(\boldsymbol{r}, t)}{c^2}\frac{\delta n_e}{n_e}A(\boldsymbol{r}, t), \tag{22}$$

where δn_e represents a plasma density modulation driven by the ponderomotive force of the laser pulse, i.e., a plasma wakefield.[37] The density modulation δn_e is responsible for electromagnetic pulse (EMP) radiation in the terahertz regime and is discussed in the following section.

2.2.6. Relativistic quiver motion. The term $S_{\rm rel}$ is due to relativistic effects arising from quiver motion of plasma electrons in the field of the laser and is given by[40]

$$S_{\rm rel}(\boldsymbol{r}, t) = -\frac{\omega_p^2(\boldsymbol{r}, t)}{4c^2}\left[\frac{q|A(\boldsymbol{r}, t)|}{mc\omega_0}\right]^2 A(\boldsymbol{r}, t). \tag{23}$$

This relativistic source term defines a critical self-focusing power due to plasma,[35,36] $P_p = 2c(q/r_e)^2 n_0(\omega_0/\omega_p)^2$, where $r_e = q^2/mc^2$ is the classical electron radius. The total nonlinear self-focusing power $P_{\rm NL}$ consists of contributions from the Kerr effect P_K, the relativistic effect P_p, and Raman scattering P_R and is given by $P_{\rm NL}^{-1} = P_K^{-1} + P_p^{-1} + P_R^{-1}$, or $P_{\rm NL} = P_p P_R P_K/(P_p P_R + P_K P_p + P_K P_R)$. For a top-hat laser pulse, a critical power due to the Raman effect can be defined in a manner similar to that for the Kerr effect .

2.2.7. Photoionization. Finally, the term describing the depletion of laser energy due to ionization is given by[40]

$$S_{\rm ion}(\boldsymbol{r}, t) = -8\pi i k_0 \frac{U_{\rm ion}}{c}\frac{\partial n_e}{\partial t}A(\boldsymbol{r}, t), \tag{24}$$

where $U_{\rm ion}$ is the characteristic ionization energy. For example, the ionization energy for O_2 is 12.1 eV, while for N_2 it is 15.6 eV.

2.3. Three-dimensional nonlinear propagation equation

Substitution of the source terms into Eq. (3) results in the following nonlinear propagation equation for the laser envelope:

$$\left[\nabla_\perp^2 + \Delta K^2 - \frac{\omega_p^2}{c^2}(1 - i\nu_e/\omega_0) + 2ik_0\frac{\partial}{\partial z} + 2i\frac{\omega_0}{c}(1-\alpha_1/2)\frac{\partial}{\partial ct} - (1-\alpha_2)\frac{\partial^2}{\partial c^2t^2} + i\alpha_3\frac{c}{\omega_0}\frac{\partial^3}{\partial c^3t^3}\right]A(\boldsymbol{r},t)$$
$$= -\left[\frac{2\omega_0^2}{c^2}(\delta n_T + \delta n_{\mathrm{TB}})n_0 + \frac{\omega_0^2 n_0^2 n_2}{4\pi c}|A|^2 + \frac{\omega_p^2}{\omega_0^2}\frac{q^2|A|^2}{4m^2c^4} - \frac{\omega_p^2}{c^2}\frac{\delta n_e}{n_e} - 8\pi i k_0 U_{\mathrm{ion}}\frac{\partial n_e}{\partial ct} + 4\pi\frac{\omega_0^2}{c^2}\chi_L Q(t)\right]A(\boldsymbol{r},t), \tag{25}$$

where the summation in Eq. (5) has been limited to $\ell \le 3$ and $\Delta K^2 = (1-\alpha_0)\omega_0^2/c^2 - k_0^2$.

It proves useful to transform the independent variables from z, t to z, τ, where $\tau = t - z/v_g$ and v_g will be set equal to the linear group velocity of the pulse. In terms of the new variables the derivatives transform as $\partial/\partial t \to \partial/\partial\tau$ and $\partial/\partial z \to \partial/\partial z - v_g^{-1}\partial/\partial\tau$. The wavenumber k_0 and group velocity v_g are as yet unspecified. It is convenient to choose them so that the form of the propagation equation is simplified. This is accomplished by setting $\Delta K = 0$ and $\Delta\Omega \equiv (1-\alpha_1/2)\omega_0 - \beta_g^{-1}ck_0 = 0$, where $\beta_g = v_g/c$. The choice $\Delta\Omega = 0$ defines the carrier wavenumber and linear group velocity, respectively, as $k_0 = (1-\alpha_0)^{-1/2}\omega_0/c = n_0\omega_0/c$ and $v_g = cn_0/(1-\alpha_1) = c/(n_0 + \omega_0\partial n_0/\partial\omega_0)$. With $\Delta K = \Delta\Omega = 0$, the final nonlinear propagation equation simplifies to

$$\left[\nabla_\perp^2 - \frac{\omega_p^2}{c^2}(1 - i\nu_e/\omega_0) + 2ik_0\frac{\partial}{\partial z} - \frac{2}{\beta_g}\frac{\partial^2}{\partial z\partial c\tau} - c^2k_0\beta_2\frac{\partial^2}{\partial c^2\tau^2} + i\alpha_3\frac{c}{\omega_0}\frac{\partial^3}{\partial c^3\tau^3}\right]A(x,y,z,\tau)$$
$$= -\left[\frac{2\omega_0^2}{c^2}(\delta n_T + \delta n_{\mathrm{TB}})n_0 + \frac{\omega_0^2 n_0^2 n_2}{4\pi c}|A|^2 + \frac{\omega_p^2}{\omega_0^2}\frac{q^2|A|^2}{4m^2c^4} - \frac{\omega_p^2}{c^2}\frac{\delta n_e}{n_e} + 8\pi i k_0\frac{U_{\mathrm{ion}}}{|A|^2}\frac{\partial n_e}{\partial c\tau} + 4\pi\frac{\omega_0^2}{c^2}\chi_L Q(t)\right]A(x,y,z,\tau). \tag{26}$$

Equation (26) describes the 3D nonlinear evolution of the complex laser field amplitude, $A(x, y, z, \tau)$. The self-consistent model employed here involves the solution of Eq. (26) along with equations that describe the response of the medium (air) to the laser field. The linear response in Eq. (26) is obtained from Eqs. (5) and (7). The nonlinear source terms are obtained by making use of Eqs. (15), (18), (19), and (21)–(24).

A 3D numerical simulation based on solving Eq. (26) together with the medium response has been developed that places the laser pulse on a Cartesian (x, y, τ) grid, allowing for the modeling of asymmetric pulse shapes and laser filamentation. The laser pulse is advanced in z according to Eq. (26) using a split-step method in which the linear terms are advanced in Fourier space, while the nonlinear terms are handled in coordinate space.[1] The equations

describing ionization, wakefield generation, and Raman scattering are solved at each z step by a fourth-order Runge–Kutta integration.

3. EMP Generation

Electromagnetic radiation has been observed originating from plasma filaments that are generated by intense laser pulses propagating in air. The EMPs have a frequency in the subterahertz range.

The wave equation for the electric field $\boldsymbol{E}$ of the EMP is given by

$$\nabla \times \nabla \times \boldsymbol{E} + \frac{1}{c^2}\frac{\partial^2 \boldsymbol{E}}{\partial t^2} = -\frac{4\pi}{c^2}\frac{\partial \boldsymbol{J}}{\partial t}, \tag{27}$$

where $\boldsymbol{J}$ is the low frequency electron current density, given by

$$\frac{\partial \boldsymbol{J}}{\partial t} + \nu_e \boldsymbol{J} = \frac{\omega_p^2(\boldsymbol{r}, t)}{4\pi}\boldsymbol{E} - \frac{q}{16\pi m}\frac{\omega_p^2(\boldsymbol{r}, t)}{\omega_0^2 + \nu_e^2}\left(\frac{\partial}{\partial z} - \frac{2\nu_e}{c}\right)|A(\boldsymbol{r}, t)|^2 \hat{\boldsymbol{e}}_z, \tag{28}$$

where $\boldsymbol{J} = qn_p\boldsymbol{V}$, q is the electron charge, n_p is the electron plasma density, $\boldsymbol{V}$ is the electron fluid velocity, ν_e is the electron collision frequency, $\omega_p^2(\boldsymbol{r}, t) = 4\pi q^2 n_p(\boldsymbol{r}, t)/m$ is the plasma frequency, and $\hat{\boldsymbol{e}}_z$ is a unit vector along the z axis. The first term on the right-hand side of Eq. (28) is associated with collective effects, and the last term represents the axial ponderomotive force due to axial gradients of the laser envelope and due to electron collisions. In this idealized model only an axial ponderomotive force exists when the spot size of the pump pulse is large compared to the plasma filament spot size. A more general description of EMP generation can be found in Ref. 41. When ionization and recombination are present the plasma density is given by

$$\frac{\partial n_p}{\partial t} + q^{-1}\nabla \cdot \boldsymbol{J} = \nu_{\text{ion}} n_n - \beta_{\text{recom}} n_p^2, \tag{29}$$

where ν_{ion} is the ionization rate, β_{recom} is the recombination rate, and n_n is the neutral density. The recombination time is $\tau_{\text{recom}} = 1/\beta_{\text{recom}} n_e$, where $\beta_{\text{recom}} \approx 2 \times 10^{-8}/\bar{T}_e^{1/2}$ [eV] cm^3/s. For $n_e = 10^{16}$ cm^{-3} and $\bar{T}_e = 1$ eV, we find that the recombination time is $\tau_{\text{recom}} \approx 5$ ns. The electron collision frequency is a function of the electron temperature. The ions are assumed to be stationary and created by the ionization process.

For azimuthally symmetric ($\partial/\partial\theta$) plasma filaments and optical pulses the axial and radial components of the electric field wave equation are given by

$$\left[\frac{1}{r}\frac{\partial}{\partial r}\left(r\frac{\partial}{\partial r}\right) - \frac{1}{c^2}\frac{\partial^2}{\partial t^2} - \frac{\omega_p^2(r, z, t)}{c^2}\right]E_z - \frac{1}{r}\frac{\partial}{\partial r}\left(r\frac{\partial E_r}{\partial z}\right)$$

$$= -\frac{q}{4mc^2}\frac{\omega_p^2(r, z, t)}{\omega_0^2}\frac{\partial}{\partial z}|A(\boldsymbol{r}, t)|^2, \tag{30a}$$

$$\left[\frac{\partial^2}{\partial z^2} - \frac{1}{c^2}\frac{\partial^2}{\partial t^2} - \frac{\omega_p^2(r, z, t)}{c^2}\right]E_r = \frac{\partial^2 E_z}{\partial r \partial z}, \tag{30b}$$

where we have assumed that $\nu_e = 0$.

To illustrate the application of Eqs. (27)–(30), generation of EMP radiation from a laser pulse propagating with velocity V equal to the group velocity in a preformed collision-less

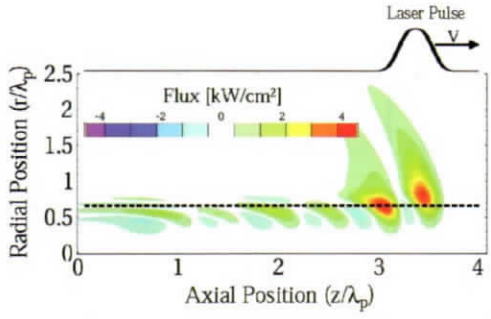

Fig. 3. Shaded contour plots of axial component of EMP Poynting flux $S_z = c(\boldsymbol{E}_L \times B_L)_z/4\pi$ in r–z plane generated by a laser pulse propagating along the axis of a plasma channel. Ratio of the channel radius to the plasma wavelength $R_{\rm ch}/\lambda_p = 2/\pi$.

plasma channel in air has been studied. The plasma channel is assumed to have cylindrical symmetry, and Eqs. (27)–(30) are numerically solved on a grid in r–z geometry for a laser pulse propagating along the axis of the channel. A shaded contour plot, in the r–z plane, of the axial component of the Poynting flux $S_z = c(\boldsymbol{E}_L \times \boldsymbol{B}_L)_z/4\pi$ is shown in Fig. 3. In this example the peak plasma density (on axis) is 10^{17} cm^{-3}, the peak laser intensity is 4×10^{13} W/cm^2, and the ratio of the channel radius to the plasma wavelength $R_{\rm ch}/\lambda_p = 2/\pi$. The flux is concentrated around two points (peak flux $\sim$4 kW/cm^2) in the trailing half of the laser pulse and around the channel boundary. Outside the channel the contours curve toward the back as the distance from the channel boundary increases. An important observation is that the axial flux is modulated at nearly one-half the plasma wavelength.

Analysis of EMP generation is simplified by transforming from z, t to z, τ variables. It can be shown that in general there is radiative EMP in the radial direction. However, in steady state (i.e., setting $\partial/\partial z \to 0$) there is no radiative EMP in the radial direction in the absence of collisions.[41] Some recent publications on the subject of EMP generation fail this important consistency check.

4. Application to a Megawatt-Class FEL Beam

In this section results from numerical solutions of Eq. (26) are presented. For many directed energy applications a 1-μm-wavelength FEL with peak (average) power in the gigawatt (megawatt) range would be a suitable source. A typical pulse format of such an FEL with a duty factor of 10^{-3} is shown in Fig. 4. In the simulations the micropulse structure of the laser beam is taken into account approximately by writing the source term in the thermal blooming equation [given following Eq. (16)] as $\alpha\langle I\rangle$, where the average intensity $\langle I\rangle$ is the peak intensity multiplied by the duty factor. The optical Kerr contribution $n_K = 5.6 \times 10^{-19}$ cm^2/W to the refractive index for air is taken into account, and thus the nonlinear power for self-focusing is $P_{\rm NL} \approx 2.8$ GW. Raman scattering is neglected in the simulations.[30]

The purpose of the first example is to show the effect of nonlinear self-focusing on laser beam propagation and, in particular, its impact on thermal blooming. With a peak intensity $I = 500$ MW/cm^2 and a spot size w_0 equal to 1.9 cm, the peak power $P = \pi w_0^2 I/2 = 2.8$ GW is at the threshold for self-focusing. A cross wind, along the positive x axis, with velocity

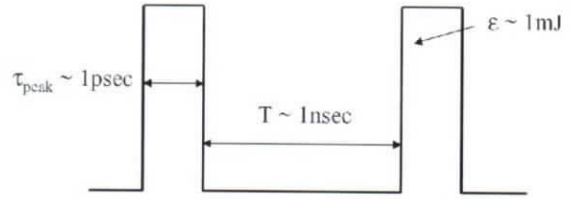

Fig. 4. Typical pulse train format of a megawatt-class FEL, with ~1-mJ energy in a micropulse.

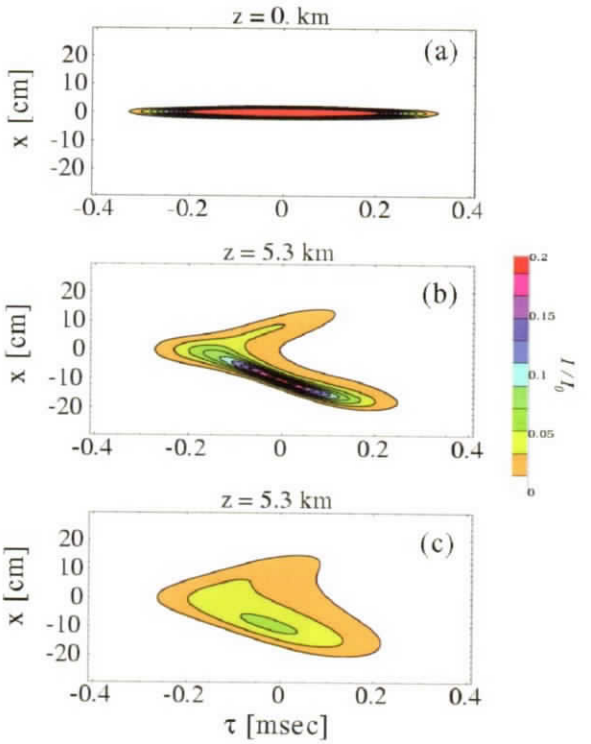

Fig. 5. Shaded contour plots of laser intensity illustrating the effect of optical Kerr self-focusing on transient thermal blooming of a laser pulse propagating in air. (a) Initial pulse in $(x-\tau)$ plane. Plots (b) and (c) show the pulse after propagating 5.3 km with and without the effect of self-focusing, respectively.

$V_w = 40$ m/s is present, and the extinction coefficient $\alpha_{\text{ext}} = 10^{-3}$ km^{-1}. Figure 5 shows contour plots of laser intensity for a beam propagating up to a distance of 5.3 km. In Fig. 5c self-focusing has been artificially turned off. Comparison of Figs. 5b and 5c shows that a significantly more intense laser beam is obtained as a result of self-focusing. This is an example of whole-beam self-focusing. (When the power exceeds the critical power significantly, the laser beam breaks up into two or more filaments.[43])

For the second example the peak intensity is dropped to $I = 20$ MW/cm^2 and the spot size w_0 is correspondingly increased to 9.4 cm to maintain the peak power at the threshold

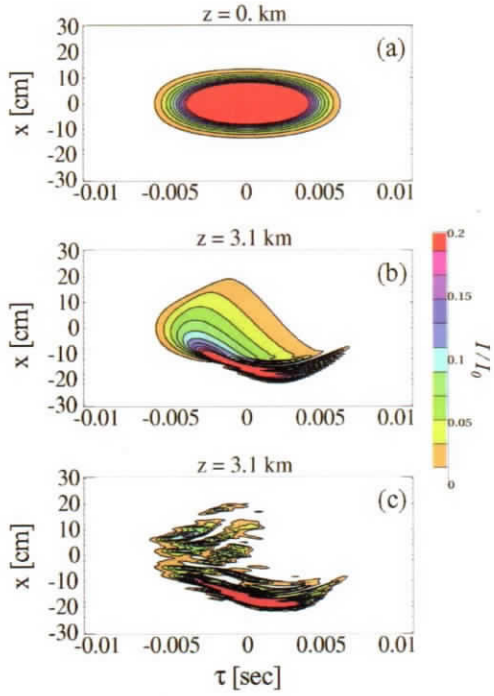

Fig. 6. Shaded contour plots of laser intensity illustrating the effect of turbulence on thermal blooming of a laser pulse propagating in air. (a) Initial pulse in (x–τ) plane. Plots (b) and (c) show the pulse after propagating 3.1 km without and with turbulence, respectively.

for self-focusing. The much smaller intensity in this example implies that the optical Kerr effect is less significant than in the previous example. A cross wind, along the positive x axis, with velocity $V_w = 30$ m/s is present, and the extinction coefficient $\alpha_{\text{ext}} = 10^{-5}$ km^{-1}. This example is used to illustrate the effect of turbulence on thermal blooming, by comparing a case without turbulence with one with a moderate amount of turbulence. In Fig. 6b the refractive index structure constant $C_n^2 = 10^{-14}$ m$^{-2/3}$, the outer scale length $L_0 = 100$ m, and the inner scale length $l_0 = 1$ cm. Comparison of Figs. 6b and 6c shows that even a moderate amount of turbulence can compromise the integrity of the beam after a few kilometers.

The last example is chosen to illustrate what is to be expected in a typical case when all the physical processes discussed in the paper and modeled by Eq. (26) are included. The parameters for this run, the results of which are shown in Figs. 7 and 8, are wind velocity $V_w = 10$ m/s, refractive index structure constant $C_n^2 = 10^{-16}$ m$^{-2/3}$ (typical value for weak turbulence), outer scale length $L_0 = 100$ m, inner scale length $l_0 = 2$ cm, extinction coefficient $\alpha_{\text{ext}} = 10^{-3}$ km^{-1}, and GVD parameter $\beta_2 = 10^{-31}$ s^2/cm. With a peak intensity $I = 5$ MW/cm^2 and a spot size radius equal to 10 cm, the peak power $P = 0.8$ GW is less than P_{NL}, and thus the laser beam should not self-focus. However, as the sequence of transverse (x–y) plane plots in Fig. 8 clearly shows, rather than whole-beam self-focusing, the beam breaks up into several hot spots after propagating nearly 4 km. With increasing propagation distance, the beam cross section is dominated by a few irregularly shaped regions of high intensity.

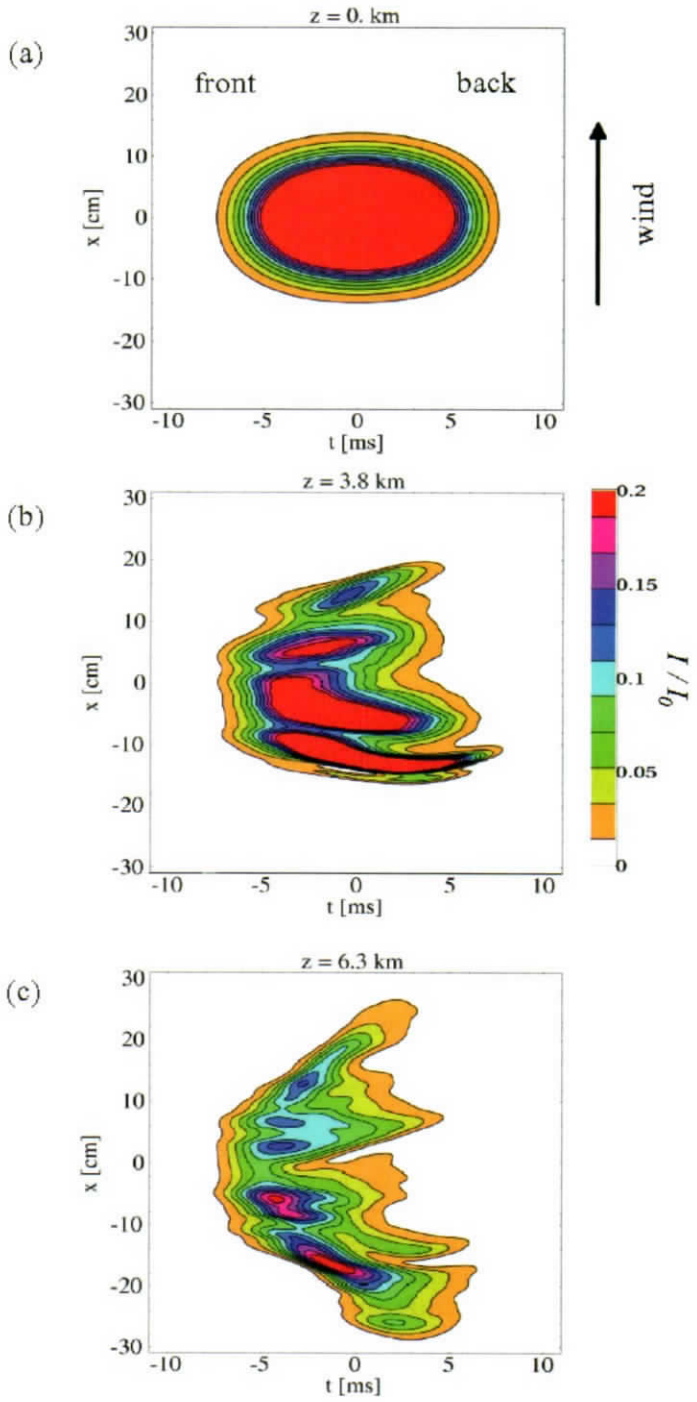

Fig. 7. Shaded contour plots of laser beam intensity in the $(t–x)$ plane at propagation distances z = (a) 0, (b) 3.8, and (c) 6.3 km through air for an FEL beam with peak intensity 5 MW/cm^2.

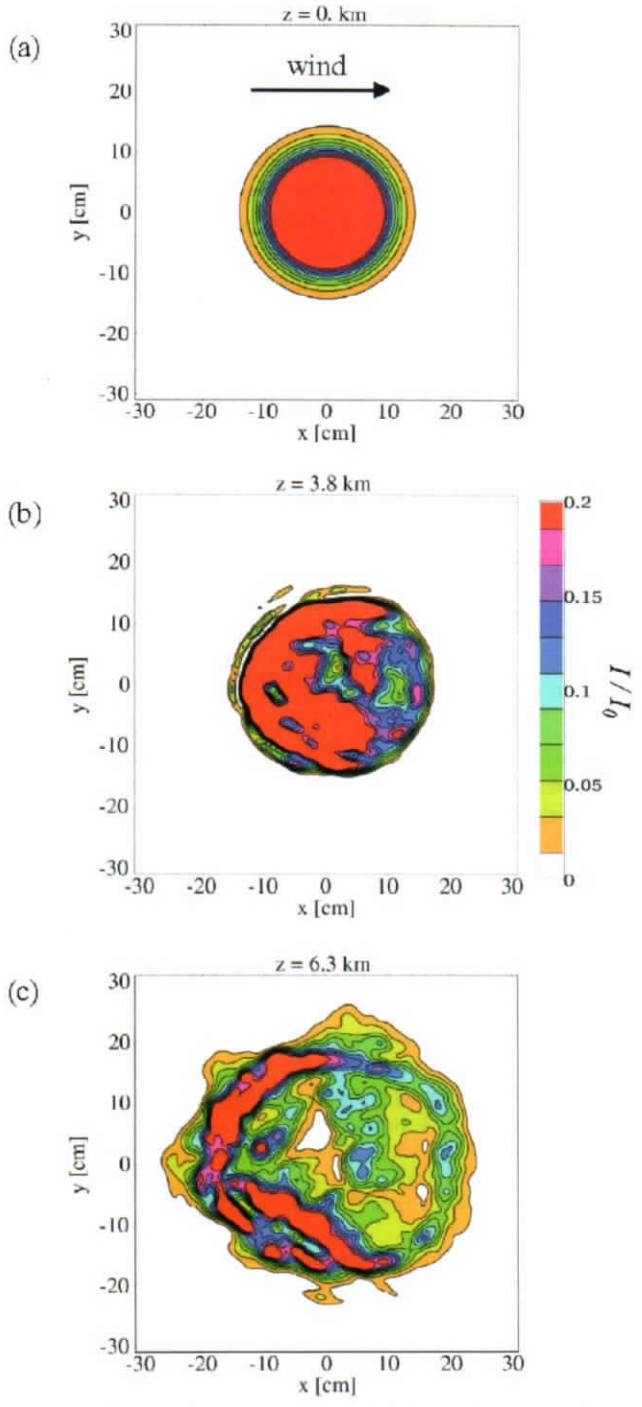

Fig. 8. Shaded contour plots of laser beam intensity in the $(x–y)$ plane at propagation distances z = (a) 0, (b) 3.8, and (c) 6.3 km through air for an FEL beam with peak intensity 5 MW/cm^2.

5. Conclusions

The central result of this paper is a 3D equation describing the nonlinear propagation of a laser pulse in the atmosphere. A discussion of the key processes affecting short-pulse, intense laser beam propagation in the atmosphere is given. The propagation model includes the effects of linear processes responsible for dispersion, absorption, scattering, and turbulence. In addition, the nonlinear processes modeled are thermal blooming, optical Kerr effect, Raman scattering, ionization, plasma response, wakefields, and relativistic quiver motion. The 3D nonlinear propagation equation is employed to study a range of problems and applications. These include guided propagation of laser energy and generation of subterahertz (EMP) radiation from femtosecond optical filaments in air. Based on the formalism it can be shown that in steady state and in the absence of collisions there is no radial flux of EMP radiation. Finally, the propagation model can be readily employed to study propagation characteristics of laser pulse trains from megawatt-class FELs.

6. Acknowledgments

This work was supported by NAVSEA, Joint Technology Office in support of the Navy DEW Program Office, and the Office of Naval Research.

References

[1]Agrawal, G.P., *Nonlinear Fiber Optics*, 2nd Ed., Academic Press, San Diego (1995).

[2]Aközbek, N., C.M. Bowden, A. Talebpour, and S.L. Chin, Phys. Rev. E **61**, 4540 (2000).

[3]Aközbek, N., M. Scalora, C.M. Bowden, and S.L. Chin, Opt. Commun. **191**, 353 (2001).

[4]Beckers, J.M., Annu. Rev. Astron. Astrophys. **31**, 13 (1993).

[5]Beland, R.R., "Propagation Through Atmospheric Optical Turbulence," *The Infrared and Electron-Optical Systems Handbook*, Vol. 2, edited by F. G. Smith, Environmental Research Institute of Michigan, Ann Arbor, MI, and SPIE Optical Engineering Press, Bellingham, WA, Chapter 2, Eq. 2.159 (1993).

[6]Bentley, S.J., R.W. Boyd, W.E. Butler, and A.C. Melissinos, Opt. Lett. **25**, 1192 (2000).

[7]Bentley, S.J., R.W. Boyd, W.E. Butler, and A.C. Melissinos, Opt. Lett. **26**, 1084 (2001).

[8]Boyd, R.W., *Nonlinear Optics*, Academic Press, San Diego (2003).

[9]Braun, A., G. Korn, X. Liu, D. Du, J. Squier, and G. Mourou, Opt. Lett. **20**, 73 (1995).

[10]Buck, A.L., Appl. Opt. **6**, 703 (1967).

[11]Chien, C.Y., B. La Fontaine, A. Desparois, Z. Jiang, T.W. Johnston, J.-C. Kieffer, H. Pepin, F. Vidal, and H.P. Mercure, Opt. Lett. **25**, 578 (2000).

[12]Coles, W.A., J.P. Filice, R.G. Frehlich, and M. Yadlowsky, Appl. Opt. **34**, 2089 (1995).

[13]Comtois, D., C.Y. Chien, A. Desparois, F. Genin, G. Jarry, T.W. Johnston, J.-C. Kieffer, B. La Fontaine, F. Martin, R. Mawassi, H. Pepin, F.A.M. Rizk, F. Vidal, P. Couture, H.P. Mercure, C. Potvin, A. Bondiou-Clergerie, and I. Gallimberti, Appl. Phys. Lett. **76**, 819 (2000).

[14]Fleck, J.A., J.R. Morris, and M.D. Feit, Appl. Phys. **10**, 129 (1976).

[15]Frehlich, R., Appl. Opt. **39**, 393 (2000).

[16]Hamster, H., A. Sullivan, S. Gordon, W. White, and R.W. Falcone, Phys. Rev. Lett. **71**, 2725 (1993).

[17]Hickman, A.P., and W.K. Bischel, Phys. Rev. A **37**, 2516 (1988).

[18]Hinson, D.P., Radio Sci. **21**, 257 (1986).

[19]Kasparian, J., R. Sauerbrey, D. Mondelain, S. Niedermeier, J. Yu, J.-P. Wolf, Y.-B. Andre, M. Franco, B. Prade, S. Tzortzakis, A. Mysyrowicz, M. Rodriguez, H. Wille, and L. Woste, Opt. Lett. **25**, 1397 (2000).

[20]Kosareva, O.G., V.P. Kandidov, A. Brodeur, C.Y. Chien, and S.L. Chin, Opt. Lett. **22**, 1332 (1997).

[21]Kurnit, N.A., and D.E. Watkins, "Stimulated Rotational Raman Scattering in the Atmosphere," LAUR 87-0097, Los Alamos National Laboratory (1987).

[22]Ladouceur, H.D., A.P. Baronavski, D. Lohrmann, P.W. Grounds, and P.G. Girardi, Opt. Commun. **189**, 107 (2001).

[23]La Fontaine, B., F. Vidal, Z. Jiang, C.Y. Chien, D. Comtois, A Desparois, T.W. Johnston, J.-C. Kieffer, H. Pepin, and H.P. Mercure, Phys. Plasmas **6**, 1615 (1999).

[24]Mlejnek, M., M. Kolesik, J.V. Moloney, and E.M. Wright, Phys. Rev. Lett. **83**, 2938 (1999).

[25]Mlejnek, M., E.M. Wright, and J.V. Moloney, Opt. Lett. **23**, 382 (1998).

[26]Mlejnek, M., E.M. Wright, and J.V. Moloney, Phys. Rev. E **58**, 4903 (1998).

[27]Mlejnek, M., E.M. Wright, and J.V. Moloney, Opt. Express **4**, 223 (1999).

[28]Neil, G.R., C.L. Bohn, S.V. Benson, G. Biallas, D. Douglas, H.F. Dylla, R. Evans, J. Fugitt, A. Grippo, J. Gubeli, R. Hill, K. Jordan, G.A. Krafft, R. Li, L. Merminga, P. Piot, J. Preble, M. Shinn, T. Siggins, R. Walker, and B. Yunn, Phys. Rev. Lett. **84**, 662 (2000).

[29]Nibbering, E.T., P.F. Curley, G. Grillon, B.S. Prade, M.A. Franco, F. Salin, and A. Mysyrowicz, Opt. Lett. **21**, 1 (1996).

[30]Peñano, J.R., P. Sprangle, P. Serafim, B. Hafizi, and A. Ting, J. Directed Energy **1** (2003) (in press).

[31]Proulx, A., A. Talebpour, S. Petit, and S.L. Chin, Opt. Commun. **174**, 305 (2000).

[32]Schillinger, H., and R. Sauerbrey, Appl. Phys. B **68**, 753 (1999).

[33]Shen, Y.R., *The Principles of Nonlinear Optics*, Wiley, New York (1984).

[34]Smith, D.C., Proc. IEEE **65**, 1679 (1977).

[35]Sprangle, P., E. Esarey, and B. Hafizi, Phys. Rev. Lett. **79**, 1046 (1997).

[36]Sprangle, P., E. Esarey, and B. Hafizi, Phys. Rev. E **56**, 5894 (1997).

[37]Sprangle, P., E. Esarey, and A. Ting, Phys. Rev. A **41**, 4463 (1990).

[38]Sprangle, P., and B. Hafizi, Phys. Plasmas **6**, 1683 (1999).

[39]Sprangle, P., B. Hafizi, and J.R. Peñano, Phys. Rev. E **61**, 4381 (2000).

[40]Sprangle, P., J.R. Peñano, and B. Hafizi, Phys. Rev. E **66**, 046418 (2002).

[41]Sprangle, P., J.R. Peñano, B. Hafizi, and C. Kapetanaka, to be published (2003).

[42]Thomas, M.E., and D.D. Duncan, "Atmospheric Transmission," *The Infrared and Electron-Optical Systems Handbook*, Vol. 2, edited by F. G. Smith, Environmental Research Institute of Michigan, Ann Arbor, MI, and SPIE Optical Engineering Press, Bellingham, WA, Chapter 1 (1993).

[43]Ting, A., D. Gordon, D. Kaganovich, E. Briscoe, C. Manka, P. Sprangle, J. Peñano, B. Hafizi, and R. Hubbard, J. Directed Energy **1** (2003) (in press).

[44]Tzortzakis, S., L. Berge, A Couairon, M. Franco, B. Prade, and A. Mysyrowicz, Phys. Rev. Lett. **86**, 5470 (2001).

[45]Tzortzakis, S., M.A. Franco, Y.-B. Andre, A. Chiron, B. Lamouroux, B.S. Prade, and A. Mysyrowicz, Phys. Rev. E **60**, R3505 (1999).

[46]Tzortzakis, S., B. Prade, M. Franco, A. Mysyrowicz, S. Hüller, and P. Mora, Phys. Rev. E **64**, 057401 (2001).

[47]Ulrich, P.B., and J. Wallace, J. Opt. Soc. Am. **63**, 8 (1973).

[48]Wöste, L., C. Wedekind, H. Wille, P. Rairoux, B. Stein, S. Nikolov, C. Werner, S. Niedermeier, F. Ronneberger, H. Schillinger, and R. Sauerbrey, Laser Optoelektron **29**, 51 (1997).

[49]Yu, J., D. Mondelain, G. Ange, R. Volk, S. Niedermeier, J.P. Wolf, J. Kasparian, and R. Sauerbrey, Opt. Lett. **26**, 533 (2001).

[50]Yugami, N., T. Higashiguchi, H. Gao, S. Sakai, K. Takahashi, H. Ito, and Y. Nishida, Phys. Rev. Lett. **89**, 065003 (2002).

[51]Zhao, X.M., J.-C. Diels, C.Y. Wang, and J.M. Elizondo, IEEE J. Quant. Electron. **31**, 599 (1995).

The Authors

Dr. Daniel F. Gordon received B.S. and Ph.D. degrees in electrical engineering from the University of California, Los Angeles, in 1991 and 1999. He joined the NRL Beam Physics Branch in 2002. He conducts research on atmospheric propagation of intense laser pulses, nonlinear laser–plasma interactions, plasma-based accelerators, and the dynamics of intense electron beams. He authored a large-scale, parallel particle-in-cell code for simulating laser–plasma interactions and maintains an active interest in numerical algorithms and high-performance computing. Prior to joining NRL, he conducted research at Rutherford–Appleton Laboratories, held a National Research Council postdoctoral fellowship, and was employed by Icarus Research, Inc.

Dr. Bahman Hafizi received B.Sc. and Ph.D. degrees in physics from Imperial College, London, in 1974 and 1978. He is president of Icarus Research, Inc. He was previously a Research Associate in the Department of Astro-Geophysics at the University of Colorado and a Staff Scientist for SAIC. His research areas include propagation of ultraintense laser pulses, laser-driven electron accelerators, laser-plasma interactions, nonlinear optics, advanced sources of electromagnetic radiation with application to imaging, lithography, and remote sensing. He is an Associate of the Royal College of Science and a member of the American Physical Society, the European Physical Society, and IEEE.

Dr. Joseph R. Peñano received B.S. and Ph.D. degrees in plasma physics from the University of California, Los Angeles, in 1991 and 1998. He joined the NRL Beam Physics Branch in 2001. He conducts research on atmospheric propagation of ultrashort, high-intensity laser pulses for directed energy weapons and electronic countermeasure applications, advanced radiation sources, and laser-driven particle accelerators. He is the chief developer of HELCAP (High Energy Laser Code for Atmospheric Propagation). Prior to joining NRL, he was employed by LET Corp. and held a National Research Council postdoctoral fellowship. He received the NRL Alan Berman Publication Award in 2003.

Dr. Phillip Sprangle received his Ph.D. in applied physics from Cornell University in 1973. He is Chief Scientist and Head of the Beam Physics Branch at NRL. His research areas include atmospheric laser propagation, free-electron lasers, and laser acceleration physics. Dr. Sprangle is a fellow of the American Physical Society and the IEEE. He won the International Free Electron Laser Prize (1991), E.O. Hulburt Science and Engineering Award (1986), and Sigma Xi Pure Science Award (1994), as well as numerous publication awards. He has published more that 200 refereed scientific articles (28 letters), and holds 12 U.S. invention patents.

Dr. Antonio C. Ting received his Ph.D. degree in physics from the University of Maryland in 1984. He is a senior research physicist and the group leader of the High Field Physics Laboratory in the Plasma Physics Division of the Naval Research Laboratory. He conducts research on intense ultrashort pulse laser interactions with air, plasmas, and electron beams for directed energy weapons, standoff detections, electronic countermeasures, advanced x-ray sources, and particle accelerators. He is a Fellow of the American Physical Society and a member of Sigma Xi and the Directed Energy Professional Society.